JOURNAL OF COMPUTATIONAL PHYSICS 51, 107–138 (1983)

Direct Implicit Large Time-Step Particle Simulation of Plasmas

A. BRUCE LANGDON, BRUCE I. COHEN, AND ALEX FRIEDMAN

University of California, Lawrence Livermore National Laboratory, Livermore, California 94550

Received February 2, 1982; revised December 3, 1982

A recently developed implicit method for solving the set of coupled particle and field equations arising in particle-in-cell plasma simulation is described in detail. This implicit integration scheme is motivated by the desire to study efficiently low-frequency, long-wavelength plasma phenomena using a large time step. In particular, this method allows the use of a time step which is larger than the electron plasma period, when electron plasma oscillations are not of interest, and provides selective damping of the distorted remnant of the electron plasma oscillation. The implicit scheme presented here uses particle data directly without introducing fluid moment equations as an intermediary between the field and particle equations. In an electrostatic model, the essence of our scheme is a linearization of the charge density at the advanced time about an explicit approximate density and the computation of the incremental correction to the charge density that is linear in the advanced field. We are led to an elliptic field equation whose coefficients depend directly on particle data accumulated on the spatial grid in the form of an effective linear susceptibility. Prediction and iterative refinement of the solution of the implicit equations, and spatial difference representations of the equations are given. Residual restrictions on time step are described. It is demonstrated that convergence is superior when spatial differencing and filtering are done in a consistent manner.

1. INTRODUCTION

The most adaptable and reliable tools for study of complex kinetic plasma behavior are the "particle" codes. Until recently, the stability of these codes required resolution of the electron plasma period in the time integration, even when the phenomena under study took place on a much longer time scale. There has been a recent advance in particle simulation as the result of the introduction of implicit time integration schemes [1–3].

The need for implicit time integration to relax time-step constraints in particle codes has long been recognized and was analyzed theoretically [4]. There has been considerable experience accumulated in the implicit time integration of the equations of fluid flow, diffusion, chemical kinetics, magnetohydrodynamics, and many other fields. However, application of such methods to particle simulation had been inhibited by the very large number of nonlinear equations to be solved simultaneously, proportional to the number of particles plus the number of zone quantities (electric and magnetic fields). Mason [1] and Denavit [2] overcome these difficulties by

0021-9991/83 $3.00

introducing fluid moment equations for mass and momentum as intermediaries between the particle equations of motion and the field equations.

Another class of methods found to improve the efficiency of particle codes takes direct advantage of the multiple time scales typically present in plasma physics. In an algorithm using electron sub-cycling [5], ions are advanced with a large time step much less often than the electrons are advanced and Poisson's equation is solved. The cost of advancing the ions thus becomes negligible in the simulation. In an orbit-averaged magneto-inductive algorithm [6], particles are advanced with a small time step that accurately resolves their orbits. An explicit solution for the electromagnetic fields, dropping radiation and electrostatics, is obtained using a current density that is accumulated from the particle data and temporally averaged over the fast, orbital time scale. Orbit-averaging reduces the number of particles required in the simulation. However, in order to apply orbit-averaging to a model including electrostatic fields and extend the simulation to long time steps, an implicit field solution must be performed [7].

Our approach to the implementation of implicit integration differs significantly from the implicit moment method. We do *not* introduce auxiliary equations. In an electrostatic model, the essence of our scheme is a linearization of the charge density at the advanced time about an explicit approximate density and the computation of the incremental correction to the charge density that is linear in the advanced field. We are led to an elliptic field equation whose coefficients depend directly on particle data accumulated on the spatial grid in the form of an effective linear susceptibility. The rank of the matrix equation is determined by the number of field quantities defined on the zones, independent of the number of particles, and normally is much smaller than the number of particles. Furthermore, the matrix equation is sparse and well-conditioned, so that solution is convenient with standard methods. Once the fields are known, the particle coordinates can be readily solved for serially, one particle at a time. We introduced this implicit method in [3] with some examples of its use. We considered the stability, accuracy, and synthesis of various time integration schemes for electrostatic particle simulation in [8]; this analysis has guided the design of algorithms that retain desirable dissipation of high-frequency oscillations while minimizing unwanted cooling of the plasma and damping of low-frequency oscillations.

This paper greatly elaborates and extends the introductory discussion of the electrostatic case in [3]. The theory underlying the direct implicit particle method and various options and restrictions in algorithm design are set forth here. The algorithm in its most elementary form is presented in Section 2, where several examples of time integration schemes and solution of the implicit field equation are described. A more detailed discussion of the solution of the implicit equations is given in Section 3. This includes the iterative refinement of the predicted field, a simple predictor version, the problem of consistent spatial filtering, restrictions on time step that limit the direct implicit particle method (as well as the moment method), and convergence of the iteration scheme. An ad hoc spatial differencing of the elliptic field prediction equation leads to a sparse banded symmetric matrix equation.

In Section 4, strict application of our approach provides difference equations with improved convergence. This is a desirable feature insofar as it leads to a more robust code. We show how the implicit contribution to the charge density can be expressed as the divergence of a polarization, introduce the susceptibility, and formulate Hamiltonian and standard cloud-in-cell linear weighting versions in one and two dimensions. The field equation is constructed using a linearization of the actual force calculation, so that its solution attempts to ensure that the finite-difference Poisson equation is satisfied. We consider the computational complexity of this "strict" formulation, and compare to the less conservative differencing of Section 3.4. A summary is given and future research directions are outlined in Section 5. The direct implicit and moment implicit methods are related and compared in Appendix A.

The selective reader may find Section 4 and Appendices B and C to be of secondary interest.

The moment equation formulation of [2] and the direct approach [3, 9] have been verified in application to ion-acoustic oscillations, two-stream instability, corona expansion into vacuum, and gravitational interchange instability, where results have already been obtained by conventional methods whose reliability is known but are much less efficient in these problems. The moment equation method is being applied to electron transport [10, 11], and to two-dimensional simulation of low-frequency instabilities and shocks [12]. A direct method is being applied to low-frequency instabilities in magnetically confined plasmas and space-physics applications [9].

2. Algorithm in Simplest Form

2.1. *Time Integration Examples*

The first major issue is the choice of finite-differenced equations of motion for the particles which have the necessary stability at large time step and are accurate for the low-frequency phenomena to be studied. A class whose application to plasma simulation has been analyzed in detail in [4] and in our present work [8] can be written in the form

$$\frac{\mathbf{x}_{n+1}-\mathbf{x}_n}{\Delta t} = c_0(\mathbf{a}_{n+1}-\mathbf{a}_n)\Delta t + c_1(\mathbf{a}_n-\mathbf{a}_{n-1})\Delta t + \cdots + \mathbf{v}_{n+1/2}, \tag{1a}$$

$$\frac{\mathbf{v}_{n+1/2}-\mathbf{v}_{n-1/2}}{\Delta t} = \mathbf{a}_n. \tag{1b}$$

These class "C" schemes damp unwanted high-frequency oscillations, while low frequencies are very weakly damped, as desired: $(\mathrm{Im}\,\omega)/\omega = \mathcal{O}(\omega\,\Delta t)^3$. Denavit's scheme [2] is a member of this class, as is Mason's centered scheme [1].

We have devised a second set of schemes [8], class "D," of the form

$$d_0(\mathbf{v}_{n+1/2} - \mathbf{v}_{n-1/2}) + d_1(\mathbf{v}_{n-1/2} - \mathbf{v}_{n-3/2}) + \cdots = \mathbf{a}_{n+1}\,\Delta t, \tag{2a}$$

$$\mathbf{x}_{n+1} - \mathbf{x}_n = \mathbf{v}_{n+1/2}\,\Delta t. \tag{2b}$$

With appropriate constraints on the coefficients $\{d_n\}$, this class has the same order of accuracy as class C. The presence of the acceleration at only the $n+1$ time level increases the damping of high-frequency oscillations. The optimum design of these difference equations is the first issue in practical implementation of large time-step methods.

2.2. *Field Equations*

In all implicit schemes the new positions $\mathbf{x}_{n+1}$ depend on the accelerations $\mathbf{a}_{n+1}$ due to the electric field $\mathbf{E}_{n+1}$. But this field is not yet known, as it depends on the density ρ_{n+1} of particle positions $\{\mathbf{x}_{n+1}\}$. The solution of this large system of nonlinear, coupled particle and field equations is the other major implementation issue.

In the first method implemented for this solution, the fields at the new time level are predicted by solving coupled field and fluid equations, in which the kinetic stress tensor is approximately evaluated from particle velocities known at the earlier time. After the fields are known, the particles are advanced to the new time level, and, if desired, an improved stress tensor is calculated and the process iterated. This approach has been described in detail in [1, 2].

It is also practical to predict the future electric field $\mathbf{E}_{n+1}$ quite directly by means of a linearization of the particle-field equations. One form of this method, its implementation, and some examples verifying its performance, have been outlined in [3]. Another form is described in [9]. Here we present the algorithm in full generality, and consider in detail many important issues, such as spatial differencing and filtering, and iterative solution of the implicit equations, which have not previously been studied.

The position $\mathbf{x}_{n+1}$ of a particle at time level t_{n+1}, as given by an implicit time integration scheme, can be written as

$$\mathbf{x}_{n+1} = \beta\,\Delta t^2\,\mathbf{a}_{n+1} + \tilde{\mathbf{x}}_{n+1} \tag{3}$$

for unmagnetized plasma, where $0 < \beta \lesssim 1$ and $\tilde{\mathbf{x}}_{n+1}$ is the position obtained from the equation of motion with the acceleration $\mathbf{a}_{n+1}$. Our examples can be written in this general form by eliminating $\mathbf{v}_{n+1/2}$ between (1a) and (1b) or between (2a) and (2b). Since $\tilde{\mathbf{x}}_{n+1}$ depends only on positions, velocities and accelerations at times t_n and earlier, it is known. In its simplest form, the direct implicit algorithm is derived by linearization of the particle positions relative to $\tilde{\mathbf{x}}_{n+1}$.

One can regard the actual position, $\mathbf{x}_{n+1}$, as $\tilde{\mathbf{x}}_{n+1}$ plus a displacement $\delta\mathbf{x} = \beta\,\Delta t^2\,\mathbf{a}_{n+1}$. We form a charge density $\rho_{n+1}^{(0)}$ from $\{\tilde{\mathbf{x}}_{n+1}\}$; the actual charge

distribution is then $\rho^{(0)}_{n+1}$, plus the change $\delta\rho$ brought about by displacing particles by the amount $\delta\mathbf{x} = \mathbf{x}_{n+1} - \tilde{\mathbf{x}}_{n+1}$. Linearized, this increment to ρ is [4]

$$\delta\rho = -\nabla \cdot [\rho^{(0)}_{n+1}(\mathbf{x})\, \delta\mathbf{x}(\mathbf{x})]. \tag{4}$$

To the same order of approximation, the displacement $\delta\mathbf{x}(\mathbf{x})$ of all particles with $\tilde{\mathbf{x}}_{n+1} \cong \mathbf{x}$ is obtained with $\mathbf{a}_{n+1}$ evaluated at $\mathbf{x}$, i.e.,

$$\delta\mathbf{x}(\mathbf{x}) \cong \beta\, \Delta t^2 \frac{q}{m} \mathbf{E}_{n+1}(\mathbf{x}). \tag{5}$$

We then have

$$\delta\rho(\mathbf{x}) = -\nabla \cdot [\chi(\mathbf{x})\, E_{n+1}(\mathbf{x})], \tag{6}$$

where the effective susceptibility is

$$\chi(\mathbf{x}) = \beta \left[\rho^{(0)}_{n+1}(\mathbf{x}) \frac{q}{m}\right] \Delta t^2 = \beta\omega_p^2(\mathbf{x})\, \Delta t^2. \tag{7}$$

With these two source contributions, the Poisson equation becomes, in rationalized cgs units,

$$\nabla \cdot \mathbf{E}_{n+1} = \rho^{(0)}_{n+1} - \nabla \cdot (\chi \mathbf{E}_{n+1}) \tag{8}$$

or

$$-\nabla \cdot [1 + \chi]\, \nabla\phi_{n+1} = \rho^{(0)}_{n+1}. \tag{9}$$

Note that this equation depends only on the particle positions $\{\tilde{\mathbf{x}}_{n+1}\}$, and not at all on velocity information as is needed in the moment equation methods.
(For a multi-species plasma, χ and $\rho^{(0)}_{n+1}$ become sums over species.) This elliptic equation is solved by standard methods. The field $-\nabla\phi_{n+1}$ and (5) are then used to calculate the positions $\{\mathbf{x}_{n+1}\}$. This algorithm is reminiscent of the method for solution for the transverse part of $\mathbf{E}$ or the vector potential $\mathbf{A}$ in some magneto-inductive plasma simulation codes [13–15]. In the limit $\omega_p^2 \Delta t^2 \gg 1$, which is the goal of this work, we have

$$[1 + \chi] \gg 1,$$

so that the field equation is drastically altered, in the direction of reducing $\nabla\phi_{n+1}$ relative to the solution of the Poisson equation with the same source $\rho^{(0)}_{n+1}$. In the opposite limit, $\omega_p^2 \Delta t^2 \ll 1$, (9) reduces to the Poisson equation. The spatial differencing is described in Section 4.

We have shown how to refine the approximations used above by linearization about a more accurate prediction of $\mathbf{x}_{n+1}$ than $\tilde{\mathbf{x}}_{n+1}$, iteration, and a more accurate evaluation of $\delta\mathbf{x}$. These notions are described in Sections 3.1, 3.2, and Appendix C.

3. Solution of the Implicit Equations: Prediction and Iteration

When introducing the method in Section 2, we made a linear expansion relative to $\{\tilde{\mathbf{x}}_{n+1}\}$. The particle displacement $\delta\mathbf{x}$ is relative to $\tilde{\mathbf{x}}_{n+1}$, and the susceptibility χ is formed from $\{\tilde{\mathbf{x}}_{n+1}\}$. These would be the new positions $\{\mathbf{x}_{n+1}\}$ if $\mathbf{E}_{n+1}$ were to be zero; also, solution of the field equation (8) yields not an increment $\delta\mathbf{E}$ but the entire field $\mathbf{E}_{n+1}$. Therefore the field equation is, in effect, a linearization about field values $\{\mathbf{E}^{(0)}_{n+1}\}$ taken to be zero.

If we had some prediction of the future fields $\{\mathbf{E}_{n+1}\}$ we might gain accuracy by doing our expansion relative to this estimate $\{\mathbf{E}^{(r)}_{n+1}\}$ and the positions $\{\mathbf{x}^{(r)}_{n+1}\}$ obtained by using this estimate in the particle equations of motion.

An issue related to this introduction of a predictor is the desirability of being *able* to iterate to approach an exact solution of the particle-field equations as closely as desired. In this section we derive a procedure which refines an estimate $\{\mathbf{E}^{(r)}_{n+1}\}$. The procedure may be used following a predictor step, and may also be used repeatedly as an iteration. In the simplest case, i.e., the prediction $\mathbf{E}_{n+1} = 0$ followed by one "iteration," the result is the same as from the formulation developed in Section 2.

In this section we also consider convergence of the iteration, and spatial filtering in the implicit field equation, which differs in a subtle way from the filtering procedure in a conventional explicit algorithm. We next introduce a simple, ad hoc spatial differencing of the field equation that leads to a sparse symmetric matrix equation. In addition, we describe time-step restrictions that persist in our implicit algorithm and briefly consider the inclusion of a magnetic field in the model.

3.1. *Iterative Refinement*

We begin with an estimate $\{\mathbf{E}^{(r)}_{n+1}\}$ for the fields $\{\mathbf{E}_{n+1}\}$. From the equations of motion we have the positions corresponding to these fields,

$$\mathbf{x}^{(r)}_{n+1} = \beta \frac{q}{m} \Delta t^2 \, \mathbf{E}^{(r)}_{n+1}(\mathbf{x}^{(r)}_{n+1}) + \tilde{\mathbf{x}}_{n+1}, \tag{10}$$

where $\tilde{\mathbf{x}}_{n+1}$ is known in terms of present and past data. While these positions and fields labelled (r) satisfy the equations of motion, the Poisson equation is *not* satisfied. That is, defining $\rho^{(r)}_{n+1}$ as the charge density corresponding to $\{\mathbf{x}^{(r)}_{n+1}\}$, we have

$$\nabla \cdot \mathbf{E}^{(r)} \neq \rho^{(r)} \tag{11}$$

Our purpose is to eliminate this discrepancy. (We have suppressed the time subscript $n+1$ in this equation and hereafter.)

We wish to calculate an improved estimate $\{\mathbf{E}^{(r+1)}\}$ with which to calculate the $\{\mathbf{x}^{(r+1)}\}$ and corresponding $\{\rho^{(r+1)}\}$ such that

$$\nabla \cdot \mathbf{E}^{(r+1)} = \rho^{(r+1)}. \tag{12}$$

Rewrite this equation as

$$\nabla \cdot \delta \mathbf{E} - \delta\rho = \rho^{(r)} - \nabla \cdot \mathbf{E}^{(r)}, \tag{13}$$

where

$$\delta \mathbf{E} \equiv \mathbf{E}^{(r+1)} - \mathbf{E}^{(r)} \tag{14}$$

and $\delta\rho$ is due to the displacements $\{\delta \mathbf{x}\} = \{\mathbf{x}^{(r+1)} - \mathbf{x}^{(r)}\}$ which result from $\delta \mathbf{E}$. (These are changes produced by an iteration step and do not correspond to changes in some interval of time.) Note that the source term for $\delta \mathbf{E}$ is the discrepancy between $\nabla \cdot \mathbf{E}^{(r)}$ and $\rho^{(r)}$, which vanishes when the implicit equations are all satisfied.

Proceeding, we express $\delta\rho$ on the left side of Eq. (13) in terms of $\delta \mathbf{E}$. First,

$$\delta \mathbf{x} = \beta\, \Delta t^2 \frac{q}{m} \left[\mathbf{E}^{(r+1)}(\mathbf{x}^{(r+1)}) - \mathbf{E}^{(r)}(\mathbf{x}^{(r)})\right] \tag{15a}$$

$$\cong \beta\, \Delta t^2 \frac{q}{m} \left[\delta \mathbf{E}(\mathbf{x}^{(r)}) + \delta \mathbf{x} \cdot \nabla \mathbf{E}^{(r)}(\mathbf{x}^{(r)})\right]. \tag{15b}$$

Rearranging, we have

$$\delta \mathbf{x} \cdot \left[\mathbf{I} - \beta\, \Delta t^2 \frac{q}{m} \nabla \mathbf{E}^{(r)}(\mathbf{x}^{(r)})\right] = \beta\, \Delta t^2 \frac{q}{m} \delta \mathbf{E}(\mathbf{x}^{(r)}), \tag{16}$$

which provides a Newton–Raphson solution of Eq. (15a). However, for now we neglect the gradient term, a point we return to in Sections 3.5.2, 3.6, and Appendix C. This leaves

$$\delta \mathbf{x} \cong \beta\, \Delta t^2 \frac{q}{m} \delta \mathbf{E}(\mathbf{x}^{(r)}). \tag{17}$$

As in Eqs. (4) and (6),

$$\delta\rho \cong -\nabla \cdot [\rho^{(r)}(\mathbf{x})\, \delta \mathbf{x}(\mathbf{x})] \cong -\nabla \cdot [\chi\, \delta \mathbf{E}], \tag{18}$$

where the susceptibility is defined in terms of $\rho^{(r)}$,

$$\chi(\mathbf{x}) = \beta \rho^{(r)}(\mathbf{x}) \frac{q}{m} \Delta t^2 = \beta \omega_p^2\, \Delta t^2. \tag{19}$$

Combining Eqs. (13) and (18), we obtain an equation for $\delta \mathbf{E}$:

$$\begin{aligned} \nabla \cdot [(1+\chi)\, \delta \mathbf{E}] &= \rho^{(r)} - \nabla \cdot \mathbf{E}^{(r)} \\ &= -\nabla \cdot (1+\chi)\, \nabla\, \delta\phi. \end{aligned} \tag{20}$$

In an electromagnetic code, implicitly differenced Faraday and Maxwell–Ampere equations could be used to obtain advanced fields. This step usually leaves $\nabla \cdot \mathbf{E} - \rho$ not quite zero. Equation (20) could then be used to refine the longitudinal part of $\mathbf{E}_{n+1}$. This correction is in the same spirit as that used in many conventional electromagnetic codes [16].

3.2. *Prediction and Iteration*

To begin the iteration, we must have a "prediction" $\mathbf{E}^{(r)}$. The trivial choice

$$\mathbf{E}^{(0)} = 0$$

with one iteration reproduces the simple algorithm of Section 2; $\rho^{(0)}$ and χ are the same, and Eq. (20), an equation for $\mathbf{E}^{(1)} = \delta\mathbf{E}$, is the same as Eq. (9). Thus the algorithm in the form given in Section 2.2 and [3] is a special case of the iterative formulation, and the option to iterate can be implemented without significantly complicating the code.

It seems likely that the field $\mathbf{E}_n$ at the preceding time is a more accurate estimate for $\mathbf{E}_{n+1}$ than zero is, at least if $\mathbf{E}$ is varying smoothly in time. Using

$$\mathbf{E}^{(0)}_{n+1} = \mathbf{E}_n$$

then locates the particles more accurately in forming ρ and χ and we expect the source term in Eq. (20), and the solution $\delta\mathbf{E}$, to be smaller. It is important to choose a time-differencing scheme which damps the Nyquist mode (odd–even in time step) if this choice for $\mathbf{E}^{(0)}$ is used.

A *linear* stability analysis with any choice of $\mathbf{E}^{(0)}_{n+1}$ recovers, as desired, exactly the same linear dispersion relations for cold plasma oscillations as those derived in [8]. However, a judicious choice for $\mathbf{E}^{(0)}_{n+1}$ improves *nonlinear* convergence; see Section 4.4.

The cycle of time integration for a predictor scheme might proceed as follows: The cycle begins after the field solve for the predicted field $\mathbf{E}^{(1)}_n$, and with $\{\mathbf{x}^{(0)}_n\}$ and $\{\mathbf{v}_{n-1/2}\}$.

- Go through particle lists.

Using $\mathbf{E}^{(1)}_n$ evaluated at $\mathbf{x}^{(0)}_n$, advance each $\mathbf{x}^{(0)}_n$, $\mathbf{v}_{n-1/2}$ to $\mathbf{x}^{(1)}_n$, $\mathbf{v}_{n+1/2}$. Using $\mathbf{x}^{(1)}_n$ and $\mathbf{v}_{n+1/2}$, calculate the temporary $\tilde{\mathbf{x}}_{n+1}$; and with $\mathbf{E}^{(0)}_{n+1} = \mathbf{E}^{(1)}_n$ evaluated at $\tilde{\mathbf{x}}_{n+1}$ extrapolate $\mathbf{x}^{(1)}_n$ to $\mathbf{x}^{(0)}_{n+1}$ collecting $\rho^{(0)}_{n+1}$ and $\chi^{(0)}_{n+1}$. Replace $\mathbf{x}^{(0)}_n$ with $\mathbf{x}^{(0)}_{n+1}$ in the particle list.

- Solve

$$-\nabla \cdot [1 + \chi^{(0)}_{n+1}(\mathbf{x})]\, \nabla\phi^{(1)}_{n+1} = \nabla \cdot [\chi^{(0)}_{n+1}(\mathbf{x})\, \mathbf{E}^{(0)}_{n+1}] + \rho^{(0)}_{n+1}$$

from which $\mathbf{E}^{(1)}_{n+1} = -\nabla\phi^{(1)}_{n+1}$ which overwrites $\mathbf{E}^{(0)}_{n+1}$. This field equation was obtained by adding $\nabla \cdot [1 + \chi^{(0)}_{n+1}]\, \mathbf{E}^{(0)}_{n+1}$ to both sides of (20) and using $\mathbf{E}^{(1)}_{n+1} = \mathbf{E}^{(0)}_{n+1} + \delta\mathbf{E}_{n+1}$.

• Repeat cycle for the next time step.

We did not form $\rho_n^{(1)}$ from $\{\mathbf{x}_n^{(1)}\}$ because we do not use it for anything. Note that we need process the particle list only once per time cycle.

If an iteration is desired, the computational cycle departs from the prediction cycle after the solution for $\mathbf{E}_{n+1}^{(1)}$.

• Iterate particle equations of motion.

with $\mathbf{E}_{n+1}^{(1)}$ evaluated at $\mathbf{x}_{n+1}^{(0)}$, advance $\mathbf{x}_{n+1}^{(0)}$ to $\mathbf{x}_{n+1}^{(1)}$ using the approximation to the equation of motion,

$$\mathbf{x}_{n+1}^{(1)} = \beta \frac{q}{m} \Delta t^2 \, \mathbf{E}_{n+1}^{(1)}(\mathbf{x}_{n+1}^{(0)}) + \tilde{\mathbf{x}}_{n+1},$$

and collect $\rho_{n+1}^{(1)}$ and $\chi_{n+1}^{(1)}$. Replace $\mathbf{x}_{n+1}^{(0)}$ with $\mathbf{x}_{n+1}^{(1)}$ in the particle list.

• Solve

$$-\nabla \cdot [1 + \chi_{n+1}^{(1)}(\mathbf{x})] \nabla \phi_{n+1}^{(2)} = \nabla \cdot [\chi_{n+1}^{(1)}(\mathbf{x}) \mathbf{E}_{n+1}^{(1)}] + \rho_{n+1}^{(1)}$$

for $\phi_{n+1}^{(2)}$. Overwrite $\mathbf{E}_{n+1}^{(1)}$ with $\mathbf{E}_{n+1}^{(2)} = -\nabla \phi_{n+1}^{(2)}$.

At this point a convergence criterion is applied to decide whether to iterate further or to advance to the next time step and repeat the computational cycle beginning with a new prediction. As given here, iteration requires retention of $\tilde{\mathbf{x}}$ in the particle list. *Only one pass* is made through the particles on the prediction step and again on each iteration.

3.3. *Spatial Filtering*

Smoothing in space is often introduced in particle simulations, to reduce nonphysical effects introduced by the spatial grid [17, 18] and to reduce the strength of the Coulomb force at small distances [19]. Such smoothing is allowable in simulation of weakly collisional plasmas because their collective behavior is dominated by long-range electromagnetic forces which are not affected by a well-chosen smoothing. We wish to be able to introduce smoothing into the implicit algorithm without overly complicating the field equation to be solved.

In a conventional electrostatic plasma simulation code, the Poisson equation is often solved by Fourier transforming ρ, multiplying $\rho(\mathbf{k})$ by a function $K^{-2}(\mathbf{k})$ which is $\cong k^{-2}$, and inverse Fourier transforming to obtain $\phi(\mathbf{x})$. In this method, smoothing is trivially introduced by including an additional factor such as $e^{-k^4 a^4}$ in K^{-2}. However, this Fourier method is not directly applicable to our field equation (9) or (20) because the operator $\nabla \cdot [1 + \chi(\mathbf{x})] \nabla$ is not invariant under translation in space, as χ is position-dependent.

Quite generally we can introduce smoothing both on ρ before, and on ϕ after, the Poisson solution. We solve

$$-\nabla^2\phi = S_1\rho, \tag{21}$$

and the particle force is then

$$\mathbf{F} = -q\nabla S_2\phi, \tag{22}$$

where S_1 and S_2 are positive semi-definite smoothing operators. This is what happens in the useful intuitive viewpoint of the particles as tenuous extended clouds of charge, so that $S_1 = S_2$, and is a convolution operation [19, 20]. We now show how to introduce such operators into the field solution.

The smoothing must be included in the estimation of the change $\delta\rho$ associated with a change $\delta\phi$ in the future potential, Eq. (18), and in the use of $\delta\rho$ in the field equation (13). We now have

$$-S_1\rho^{(r)} - \nabla^2\phi^{(r)} = \nabla^2\,\delta\phi + S_1\,\delta\rho \tag{23a}$$

$$= \nabla^2\,\delta\phi + S_1\nabla\cdot[\chi\nabla S_2\,\delta\phi]$$

$$= \nabla\cdot[1 + S_1\chi S_2]\,\nabla\,\delta\phi \tag{23b}$$

$$= \nabla\cdot[S_2^{-1} + S_1\chi]\,\nabla(S_2\,\delta\phi), \tag{23c}$$

where the left-hand side is known and the right-hand side has been manipulated through several forms. We assume S_1 and S_2 commute with the divergence and gradient operators. Note that operator S_1 applies not just to χ but to $\chi S_2\nabla\,\delta\phi$. The locality of the field equation operator, and therefore the sparsity of its matrix representation, have been degraded; this complicates the solution of (23b) or (23c).

We could rely solely on S_1 and abandon S_2, but let us first try solving Eq. (23c) for $(S_2\,\delta\phi)$ instead of $\delta\phi$. After operating on Eq. (23c) with S_2, we have[1]

$$-\{S_2S_1\rho^{(r)}\} - \nabla^2\{S_2\phi^{(r)}\} = \nabla\cdot[1 + S_2S_1\chi]\,\nabla\{S_2\,\delta\phi\} \tag{24}$$

or

$$-\rho_s^{(r)} - \nabla^2\phi_s^{(r)} = \nabla\cdot[1 + S_2S_1\chi]\,\nabla\,\delta\phi_s. \tag{25}$$

We add smoothing by applying S_2S_1 to the density, $\rho_s \equiv S_2S_1\rho$, and use this in Eq. (25), whose solution is $\delta\phi_s \equiv S_2\,\delta\phi$. Then $-\nabla\phi_s^{(r+1)} = -\nabla(\phi_s^{(r)} + \delta\phi_s)$ is used to advance the particles; ϕ itself is never calculated. Handling S_2 in this manner produces the same calculational steps as if only ρ were smoothed, i.e., Eq. (23b) with $S_2 \equiv \mathbf{I}$.

[1] Note that $S_2\,\delta\phi$ *cannot* be obtained by an operation of S_2 on the solution ϕ of the unsmoothed equation (20).

It is tempting to solve Eq. (9) or (20), smooth the solution ϕ, and use this to advance the particles, but this is not consistent since the smoothing is then not taken into account in estimating $\delta\rho$ (the χ term). In Section 3.6 we show that inconsistent smoothing degrades convergence. Barnes *et al.* [9] have found in simulations that only consistent spatial smoothing in the form of (25) gave them reasonable results; analysis such as this gives useful guidance in code applications.

3.4. *Spatial Differencing and Implementation*

So far, **E** has been defined for all **x**, and we have taken gradients of **E** and other fields. In this section we describe the simplest formulation of finite difference implicit field equations that still preserves their essential features, yet requires no more computational effort for the particles than is needed in an explicit code. Section 4 develops a more rigorous formulation.

Following Eq. (4), we use a representation of $\delta\rho$ as an exact difference analogue to the divergence of a polarization $\mathbf{P} = \rho\,\delta\mathbf{x}$. In two dimensions,

$$\delta\rho_{j,k} = -\frac{P_{x,j+1/2,k} - P_{x,j-1/2,k}}{\Delta x} - \frac{P_{y,j,k+1/2} - P_{y,j,k-1/2}}{\Delta y}. \tag{26}$$

(See Fig. 1.) This is a charge-conserving representation of $\delta\rho$ in that the change δQ of the charge in a volume, which is a sum of $\delta\rho_{j,k}$, involves only **P** at the surface. (This is the difference analogue of Gauss' integral theorem.)

In one dimension, the simplest representation of $\mathbf{P} = \chi\,\delta\mathbf{E}$ is

$$P_{j+1/2} = -\chi_{j+1/2}\frac{\delta\phi_{j+1} - \delta\phi_j}{\Delta x}. \tag{27}$$

The resulting field equation couples three ϕ's in one dimension, and either five or nine ϕ's in two dimensions, depending on how the χ's are defined. Ideally we would like to calculate χ from the ρ for each species, or at least to have to accumulate no more information from the particle positions than is necessary already to form ρ, as these accumulations are computationally expensive. For example,

$$\chi_{j+1/2} = \beta\,\Delta t^2\frac{q}{m}\left(\left[\tfrac{1}{2} - \alpha_{j+1/2}\right]\rho_j + \left[\tfrac{1}{2} + \alpha_{j+1/2}\right]\rho_{j+1}\right) \tag{28a}$$

or

$$\chi_{j+1/2} = \beta\,\Delta t^2\,\max\left(\rho_j\frac{q}{m}, \rho_{j+1}\frac{q}{m}\right). \tag{28b}$$

(As usual, summation of $\rho q/m$ over species is understood.) The choice $\alpha = 0$ produces an average of ρ; perhaps α may provide useful tuning in the spirit of [21], in regions of strong gradients. If the range of α is restricted so that $1 + \chi$ remains

positive, then it is shown in Appendix B that the combination of (26)–(28) leads to a field equation with a positive matrix. The form of (28b) is motivated by preliminary results on stability with non-strict differencing which indicate that it is most important that χ not be too small.

This one-dimensional representation of P is the same as arises in Section 4.2 in a systematic construction of field equations, but $\chi_{j+1/2}$ here differs from (62). In two dimensions we could similarly express $\mathbf{P}$ in the form of (65), but form χ_x and χ_y more simply from ρ rather than as in (66).

We note that the spatial differencing of the fluid equations in the implicit moment algorithms [1, 2, 7, 12] is not exactly consistent with that of the particle and charge density equations. No difficulties in these codes have been attributed to this inconsistency, which encourages us to expect success with straightforward differencing in direct implicit methods, as has been the experience of Barnes *et al.* [9] in their two-dimensional applications when *consistent* smoothing is added.

3.5. *Restrictions*

Although we have overcome the stability limit on $\omega_p \Delta t$, there remain some restrictions which involve Δt.

Dispersion function results, such as Eq. (29) below, apply strictly only when the particle-field equations are solved exactly. Results may differ if iteration is not taken close to convergence. Ideally we prefer to process the particles only once per time step; with one iteration, the choice of starting values (Section 3.2) may become critical.

3.5.1. *Electron Transit Time Limitation on $v\,\Delta t/L$*

When a particle moves in one time step a distance greater than a scale length L for spatial variation of fields, the particle does not sample the field sufficiently closely in space to respond correctly to the field structure. This is illustrated in the case of sinusoidal field variation and a class of time integration schemes introduced in [4] and examined further in [8]. The dielectric function for this case, with finite Δt but ignoring Δx, can be written [4]

$$\begin{aligned}\varepsilon &= \varepsilon_{\text{leap-frog}} + \omega_p^2 \Delta t^2 [c_0 + c_1 e^{i\omega\Delta t} \tilde{f}_0(\mathbf{k}\,\Delta t) + c_2 e^{2i\omega\Delta t} \tilde{f}_0(2\mathbf{k}\,\Delta t) + \cdots] \\ &= 1 + \omega_p^2 \Delta t^2 \left[c_0 + \sum_{s=1} (s + c_s)\, e^{i\omega s\Delta t} \tilde{f}_0(s\mathbf{k}\,\Delta t) \right] \end{aligned} \tag{29}$$

where $c_0 \equiv \beta$, and

$$\tilde{f}_0(\tilde{\mathbf{v}}) = \int d\mathbf{v}\, f_0(\mathbf{v})\, e^{-i\mathbf{v}\cdot\tilde{\mathbf{v}}}. \tag{30}$$

For a Maxwellian velocity distribution $\tilde{f}_0(\mathbf{k}\,\Delta t) = \exp(-\frac{1}{2}k^2 v_t^2\,\Delta t^2)$, where $v_t^2 \equiv T/m$,

and the series in Eq. (29) converges quickly for $kv_t \Delta t \gtrsim 1$, the limit of present interest.

At very low frequency, as in a sound wave, we require that electrons reproduce Debye shielding, and perhaps also Landau damping,

$$\varepsilon = 1 + \frac{1}{k^2 \lambda_{\mathrm{De}}^2} + \text{resonance terms.} \tag{31}$$

For $kv_t \Delta t \gtrsim 1$, the implicit code produces instead, from (29) and (30),

$$\varepsilon \cong 1 + \omega_p^2 \Delta t^2 [c_0 + (1 + c_1) \exp(i\omega \Delta t - \tfrac{1}{2} k^2 v_t^2 \Delta t^2)]. \tag{32}$$

Comparing (31) and (32), we see that ε in the implicit code is larger by a factor $\cong \beta k^2 v_t^2 \Delta t^2$ than the correct result, when $\beta \omega_p^2 \Delta t^2 \gtrsim 1$ and $k^2 v_t^2 \Delta t^2 \gtrsim 1$. The implicit code shields too strongly at short wavelengths. Accurate shielding requires $k^2 v_t^2 \Delta t^2 \lesssim 1$. When $\omega_p^2 \Delta t^2 \gg 1$ this restricts us to wavelengths large compared to a Debye length, since

$$k\lambda_{\mathrm{D}} = \frac{kv_t \Delta t}{\omega_p \Delta t} \ll 1.$$

Unfortunately, therefore, applications such as ion-acoustic turbulence, for which $k\lambda_D \sim \frac{1}{2}$, do not benefit much from implicit integration.

At short wavelengths, from (32) we see that the implicit algorithm is at least stable, and errs in the direction of making $\delta \mathbf{E}$ too small. Thus, it appears that the presence of short wavelengths may not interfere with the longer wavelengths which are simulated accurately. Finite $kv_t \Delta t$ does not appear to affect convergence of our solution process (Section 3.1) whereas $kv_t \Delta t \gtrsim 1$ does upset convergence of the moment-implicit method [2, 22]. Also, even in the direct method, when $\mathbf{E}_{n+1}$ in (10) is evaluated at $\mathbf{x}_n$ rather than $\mathbf{x}_{n+1}^{(r)}$, a $kv_t \Delta t$ constraint reappears [9].

3.5.2. *Trapping Frequency Limitation on* $\omega_{\mathrm{tr}} \Delta t$

We now consider the magnitude of the neglected gradient term in Eq. (16) for $\delta \mathbf{x}$. In one dimension, near a minimum of $q\phi$, the term is

$$-\beta \Delta t^2 \frac{q}{m} \frac{\partial E}{\partial x} = +\beta(\omega_{\mathrm{tr}} \Delta t)^2, \tag{33}$$

where ω_{tr} is the frequency of oscillation of a particle "trapped" near the bottom of the potential well. Since β is $\mathcal{O}(1)$, we see that the neglected term is important when Δt is too large to resolve trapping oscillations.

We can express this condition in other instructive forms, e.g.,

$$(\omega_{\mathrm{tr}} \Delta t)^2 = (kv_t \Delta t)^2 \frac{q\phi}{T_e}. \tag{34}$$

As shown in the preceding section and in [8], accuracy may require $kv_t \Delta t \lesssim 1$. Also, the physics of the situation under study often limits variations in ϕ to $\lesssim T_e/q$. If both these conditions are met, then (34) shows that the trapping frequency condition is satisfied. By a similar argument,

$$(\omega_{\rm tr} \Delta t)^2 = (kv_t \Delta t) \frac{a \Delta t}{v_t}. \tag{35}$$

Presumably most particle velocities are much larger than their increment $a \Delta t$ in one time step; if so, the condition $kv_t \Delta t \lesssim 1$ is the more restrictive.

We can also rewrite the left side of (33) as

$$\beta \Delta t^2 \frac{q_e}{m_e} \frac{\partial E}{\partial x} = \beta(\omega_{\rm pe} \Delta t)^2 \frac{|\rho_{\rm net}|}{|\rho_{\rm electron}|}.$$

When $(\omega_{\rm pe} \Delta t)^2 \gg 1$, we see that the net charge imbalance must be much less than the total electron charge density, i.e., the plasma cannot be grossly non-neutral.

Let us consider briefly how the field algorithm changes if we do not neglect the term (33), and use the Newton–Raphson expressions (37) for $\delta \mathbf{x}$ and (39) for χ. Near a minimum of $q\phi$, we see that χ is reduced by the factor $|1 + \beta(\omega_{\rm tr} \Delta t)^2|$. The effect of neglecting the $\nabla \mathbf{E}$ term is to make the solution $\nabla \delta\phi$ too *small* by approximately this same factor. At a maximum of $q\phi$ such that the neglected term is >1, the denominator of (39) is negative. If $1 + \chi$ becomes negative as a result, then the operator $-\nabla \cdot (1 + \chi) \nabla$ becomes negative in this region (Appendix B), which invalidates some methods for solution of the field equation in two dimensions, and may have more serious implications. In most of this paper, except in Section 3.6, where it affects convergence, and in Appendix C, we neglect this $\nabla \mathbf{E}$ correction.

3.5.3. *Numerical Cooling or Heating*

A secular acceleration, which can artificialy cool or heat the plasma, is a side effect of damping introduced to suppress high frequencies. This effect is discussed in detail in a companion paper [8]. In brief, in the presence of a sinusoidal wave, the nonphysical acceleration scales with field strength as measured by $(\omega_{\rm tr} \Delta t)^2$, and is a function of $(\omega - \mathbf{k} \cdot \mathbf{v}) \Delta t$ whose form depends on the difference equations and is most troublesome with schemes whose damping is first order in Δt [1] rather than $\mathcal{O}(\Delta t^3)$.

3.6. *Convergence of the Iteration*

In order that the iteration improve the solution of Poisson's equation (12), successive iterations must reduce $\rho - \nabla \cdot E$ to zero. We now calculate the rate of convergence with use of Eqs. (13)–(20). Having solved (20) for $\delta \mathbf{E}^{(r+1)}$ we update position and field to $\mathbf{x}^{(r+1)}$ and $\mathbf{E}^{(r+1)}$. We compare the new residual $\rho^{(r+1)} - \nabla \cdot \mathbf{E}^{(r+1)}$ to the old, $\rho^{(r)} - \nabla \cdot \mathbf{E}^{(r)}$ (which is the source for $\delta \mathbf{E}^{(r+1)}$). The

new residual is $|\rho^{(r+1)} - \nabla \cdot \mathbf{E}^{(r+1)}| = |\rho^{(r)} - \nabla \cdot \mathbf{E}^{(r)}| + |\delta\rho^{(r+1)} - \nabla \cdot \delta\mathbf{E}^{(r+1)}|$. We use (20) to express the old residue, and (18) to express $\delta\rho$ in terms of $\delta\mathbf{x}$. The ratio is

$$\frac{|\rho^{(r+1)} - \nabla \cdot \mathbf{E}^{(r+1)}|}{|\rho^{(r)} - \nabla \cdot \mathbf{E}^{(r)}|} = \frac{|\nabla \cdot [(\chi^{(r)}\, \delta\mathbf{E}^{(r+1)}) - \rho^{(r)}\, \delta\mathbf{x}^{(r+1)}]|}{|\nabla \cdot (1+\chi^{(r)})\, \delta\mathbf{E}^{(r+1)}|}. \tag{36}$$

Now it is necessary to specify the expressions used for $\delta\mathbf{x}$ and χ.

The equation of motion (10) leads to a relation between $\delta\mathbf{x}^{(r+1)}$ and $\delta\mathbf{E}^{(r+1)}$ given in (16). In one dimension,

$$\delta x^{(r+1)} = \beta N^{-1} \frac{q}{m} \Delta t^2\, \delta E^{(r+1)}, \tag{37}$$

where $N \equiv (1 - \beta q m^{-1} \Delta t^2\, \partial E^{(r)}/\partial x)$. With $\chi^{(r)}$ given by (19),

$$\frac{|\rho^{(r+1)} - \nabla \cdot \mathbf{E}^{(r+1)}|}{|\rho^{(r)} - \nabla \cdot \mathbf{E}^{(r)}|} \cong \frac{|\nabla \cdot (N^{-1}\chi^{(r)} \beta q m^{-1} \Delta t^2\, \partial E^{(r)}/\partial x)\, \delta\mathbf{E}|}{|\nabla \cdot (1+\chi^{(r)})\, \delta\mathbf{E}^{(r+1)}|} \tag{38}$$

which we require to be less than unity for convergence. We recognize $(\omega_{\mathrm{tr}} \Delta t)^2 \equiv |q m^{-1} \Delta t^2\, \partial E^{(r)}/\partial x|$, where ω_{tr} is the electrostatic trapping frequency, in the numerator of the right side of (38); thus, convergence improves for $(\omega_{\mathrm{tr}} \Delta t)^2 \ll 1$.

If we retain the Newton–Raphson correction to the susceptibility,

$$\chi^{(r)} = \beta N^{-1} \rho^{(r)} \frac{q}{m} \Delta t^2, \tag{39}$$

then the right side of (36) *vanishes* to the order calculated, viz., through $\mathcal{O}(\omega_{\mathrm{tr}}^2 \Delta t^2)$. Provided that $\omega_{\mathrm{tr}}^2 \Delta t^2 \lesssim 1$, this significantly accelerates convergence of the iteration scheme. This condition is discussed in Section 3.5.

These convergence properties differ markedly from the convergence of the implicit moment method with explicit kinetic stress tensor, which requires $k v_t \Delta t \lesssim 1$ [1, 2, 12, 22], generally a more restrictive condition.

With consistent spatial smoothing and inclusion of the Newton–Raphson correction to χ, the residual $\rho^{(r+1)} - \nabla \cdot \mathbf{E}^{(r+1)}$ calculated as in (36) cancels through orders unity and $\beta\omega_{\mathrm{tr}}^2 \Delta t^2$. However, with either forces or charges inconsistently smoothed, cancellation of order unity terms does not occur and we obtain residuals like

$$\frac{|\rho^{(r+1)} - \nabla \cdot \mathbf{E}^{(r+1)}|}{|\rho^{(r)} - \nabla \cdot \mathbf{E}^{(r)}|} = \frac{|\nabla \cdot (\tilde{S}_2 \tilde{S}_1 - S_2 S_1)\, \chi^{(r)}\, \delta\mathbf{E}^{(r+1)}|}{|\nabla \cdot (1+\chi^{(r)})\, \delta\mathbf{E}^{(r+1)}|}. \tag{40}$$

to leading order, where $\tilde{S}_2 \tilde{S}_1 - S_2 S_1$ gives the difference of the inconsistent smoothing operators $\tilde{S}_2 \tilde{S}_1$ from consistent smoothing $S_2 S_1$. For typical smoothing

operators, convergence is most severely degraded for plasma densities and/or electric fields that vary rapidly in space.

In summary, we have demonstrated that convergence is faster than linear when the susceptibility χ in the field solve is consistent with the position increment δx in the equation of motion. This follows directly from the construction of the implicit field equation. In an actual code, retention of this property depends on how the equations are finite-differenced and on other issues; see Section 4.4.

3.7. *Magnetized Plasma*

In [8] we proposed generalizations of the class C and D schemes to include a magnetic field **B**. Here we outline how these two generalizations affect the solution for the advanced field. In one case the field equation does not change at all; in the other χ changes greatly, to a tensor which introduces an antisymmetric term into the field equation.

For class C we use (1) in which (1b) becomes

$$\frac{\mathbf{v}_{n+1/2} - \mathbf{v}_{n-1/2}}{\Delta t} = \mathbf{a}_n + \frac{\mathbf{v}_{n+1/2} + \mathbf{v}_{n-1/2}}{2} \times \boldsymbol{\Omega}, \tag{41}$$

where $\mathbf{a}_n$ is due only to the electric field and $\boldsymbol{\Omega} \equiv q\mathbf{B}/mc$. Since $\mathbf{x}_{n+1}$ depends on $\mathbf{a}_{n+1}$ only through the term $c_0\mathbf{a}_{n+1}$, χ is unaffected by the magnetic field, and the field equation is unchanged.

We next generalize the D schemes (2) to include a magnetic field. First we factor

[redacted]

equations are

$$d_0\mathbf{a}'_n + d_1\mathbf{a}'_{n-1} + \cdots = \mathbf{a}_{n+1}, \tag{42a}$$

$$\mathbf{a}'_n = \frac{\mathbf{v}_{n+1/2} - \mathbf{v}_{n-1/2}}{\Delta t} - \frac{\mathbf{v}_{n+1/2} + \mathbf{v}_{n-1/2}}{2} \times \boldsymbol{\Omega}, \tag{42b}$$

$$\frac{\mathbf{x}_{n+1} - \mathbf{x}_n}{\Delta t} = \mathbf{v}_{n+1/2}. \tag{42c}$$

These difference equations are equivalent to Eq. (35) in [8]. (This factorization has been used by Barnes and Kamimura [9, 24]. However, they apply the recursive filter to the field *defined on the grid*. Their non-Galilean invariant step changes dispersion, stability, and momentum conservation properties; see [8], Appendix B, and [9].) For simplicity we consider components perpendicular to $\boldsymbol{\Omega}$ in the limit $(\Omega\,\Delta t)^2 \gg 1$, for which the dominant terms produce the $\mathbf{E} \times \mathbf{B}$ drift. The susceptibility becomes a tensor,

$$\chi = \omega_p^2 \frac{\partial \mathbf{x}_{n+1}}{\partial \mathbf{a}_{n+1}} = -\frac{2}{d_0} \frac{\omega_p^2 \Delta t}{\Omega^2} \boldsymbol{\Omega} \times \mathbf{I}. \tag{43}$$

The corresponding term in the field equation is

$$\nabla \cdot (\chi \cdot \nabla\phi) = -\nabla \cdot \left[\frac{2}{d_0} \frac{\omega_p^2 \Delta t}{\Omega^2} \Omega \times \nabla\phi \right]. \tag{44}$$

Multiplying by another potential function ψ and integrating by parts,

$$\int d\mathbf{x}\, \psi \nabla \cdot (\chi \cdot \nabla\phi) = \int d\mathbf{x} \frac{2}{d_0} \frac{\omega_p^2 \Delta t}{\Omega^2} \Omega \cdot \nabla\phi \times \nabla\psi$$

$$= -\int d\mathbf{x}\, \phi \nabla \cdot (\chi \cdot \nabla\psi).$$

Thus this new term is antisymmetric. The differential field equation operator remains positive (however, the *difference* form requires care; see Appendix B). These considerations affect the choice of methods for solving the matrix representation.

4. Strict Spatial Difference Equations

In this section we apply our concepts of constructing a field equation using the functional derivative $\partial\rho/\partial\mathbf{E}$ to numerical algorithms actually used for the force calculation, in which ρ, ϕ, and $\mathbf{E}$ are defined on a spatial grid. A rigorous, conservative approach is taken with the spatial differencing and interpolation. For the resulting field equations we are able to give an analytic argument for convergence to solution of the coupled field and particle equations.

In our spatial-difference representation of these equations, Eq. (18) becomes the gradient of a zonal ρ with respect to particle position, and $\delta\mathbf{x}$ in Eq. (17) depends on the electric field in two zones, using the usual interpolation. In this way we are assured that the density ρ_{n+1} of final particle positions $\{\mathbf{x}_{n+1}\}$ satisfies the code's representation of the Poisson equation, $-\nabla^2\phi_{n+1} = \rho_{n+1}$, so that desirable features built into the time-differencing scheme will be realized in practice. We therefore term this a "strict" implementation. Strict differencing preserves the convergence properties derived in Section 3.6. Simplified differencing (Section 3.4) and inconsistent spatial smoothing (Section 3.3) both lead to slower convergence.

In the following we obtain specific expressions for the quantities that would be calculated in practical implementation. We consider first a Hamiltonian[2] multidimensional algorithm, which is useful as a mathematically clean prototype and study case, and is also more stable to the spatial-grid instability in [12], then a commonly used momentum-conserving algorithm. Lastly, we compare the computational complexity and convergence properties of strict and simplified schemes.

[2] These are sometimes called "energy-conserving" algorithms, although energy is conserved only for *exact* time integration [25].

4.1. *$\delta\rho$ Expressed as a Divergence*

In Section 3 we expressed $\delta\rho$ as a divergence of a polarization,

$$\delta\rho = -\nabla \cdot \mathbf{P}. \tag{45}$$

and its difference equivalent, (26). For the gridded case, we show how to evaluate $\delta\rho$ in this manner for ρ as actually collected from the particle positions. Writing $\delta\rho$ this way is particularly simple for the common linear choice of weighting function S, clarifies many later steps, and leads to a first integral of the field equation.

Let us consider why we should expect such a result more generally. The charge density is defined on the grid by

$$\rho_{\mathbf{j}} = \sum_{i} q_i S(\mathbf{X}_{\mathbf{j}} - \mathbf{x}_i), \tag{46}$$

where i and $\mathbf{j}$ are particle and grid indices and $\{\mathbf{X}_{\mathbf{j}}\}$ are the locations of the grid points. The function S is designed so that

$$V_c \sum_{\mathbf{j}} S(\mathbf{X}_{\mathbf{j}} - \mathbf{x}) \equiv 1, \tag{47}$$

for all $\mathbf{x}$, which means that

$$V_c \sum_{\mathbf{j}} \rho_{\mathbf{j}} \equiv \sum_{i} q_i \tag{48}$$

when the sums are taken over the whole system. Here, V_c is the volume of a cell, equal to Δx in one dimension. In words, the total charge on the grid is the same as the total particle charge. Therefore it does not change as a result of small displacements $\{\boldsymbol{\delta}\mathbf{x}\}$. Further, the change in the charge on the grid points within some boundary involves only the particles in cells near the boundary. These are characteristics of an integral of a divergence. In the gridded case, the integral becomes a sum in which interior contributions cancel.

We now assume, as is commonly the case, that S is a *spline* weighting function, $S_m(x)$, where S_0 is the nearest grid-point weighting, $S_1 \equiv S_0 * S_0$ ($*$ denotes convolution) is the linear weighting, $S_2 \equiv S_0 * S_0 * S_0 \equiv S_0 * S_1$ is a quadratic spline, and so on ([25, Section VII]). Proceeding for now in one dimension, we have

$$\delta\rho_j = -\sum_{i} q_i \, \delta x_i \, S'_m(X_j - x_i), \tag{49}$$

in which the derivative S'_m can be expressed in terms of the next lower-order function S_{m-1}:

$$S'_m(x) \equiv \frac{1}{\Delta x}\left[S_{m-1}\left(x + \frac{\Delta x}{2}\right) - S_{m-1}\left(x - \frac{\Delta x}{2}\right)\right]. \tag{50}$$

This result follows from the identity $S_m \equiv S_0 * S_{m-1}$. Now we can write

$$\delta\rho_j = -\frac{P_{j+1/2} - P_{j-1/2}}{\Delta x}, \tag{51}$$

the one-dimensional version of (26), with

$$P_{j+1/2} = \sum_i q_i \, \delta x_i \, S_{m-1}(X_{j+1/2} - x_i). \tag{52}$$

For the simplest and very popular case of $m = 1$ (linear weighting),

$$P_{j+1/2} = \frac{1}{\Delta x} \sum_{i \in j+1/2} q_i \, \delta x_i \tag{53}$$

is just a sum of polarizations $q\,\delta x_i$ of all particles in cell $j + \frac{1}{2}$ (i.e., $j\,\Delta x \leqslant x_i \leqslant (j+1)\,\Delta x$), normalized to be a polarization density.

In two dimensions the usual generalization of S_m is

$$S_m(x, y) = S_m(x)\, S_m(y). \tag{54}$$

The charge density at grid point (j, k), which is located at $(X_j, Y_k) \equiv (j\,\Delta x, k\,\Delta y)$, is

$$\rho_{j,k} = \sum_i q_i S_m(X_j - x_i)\, S_m(Y_k - y_i). \tag{55}$$

Using (50) for each factor of $S_m(x, y)$, the variation of $\delta\rho$ due to particle displacements is again in the form of a divergence of $\mathbf{P}$, as in (26), where now

$$P_{x,j+1/2,k} = \sum_i q_i \, \delta x_i \, S_{m-1}(X_{j+1/2} - x_i)\, S_m(Y_k - y_i), \tag{56a}$$

$$P_{y,j,k+1/2} = \sum_i q_i \, \delta y_i \, S_m(X_j - x_i)\, S_{m-1}(Y_{k+1/2} - y_i). \tag{56b}$$

The spatial relationships among ρ, P_x, P_y, etc., are illustrated in Figs. 1 and 2.

4.2. *Hamiltonian Case*

Following [17, 25], the force calculation is

$$\begin{aligned} \rho_{\mathbf{j}} &= -(\nabla^2\phi)_{\mathbf{j}} \\ &\equiv V_c \sum_{\mathbf{j}'} \phi_{\mathbf{j}'} \int d\mathbf{x} [\nabla S(\mathbf{X}_{\mathbf{j}} - \mathbf{x})] \cdot [\nabla S(\mathbf{X}_{\mathbf{j}'} - \mathbf{x})], \end{aligned} \tag{57}$$

$$\mathbf{a}(\mathbf{x}) = -\frac{q}{m} \nabla V_c \sum_{\mathbf{j}'} \phi_{\mathbf{j}'} S(\mathbf{X}_{\mathbf{j}'} - \mathbf{x}), \tag{58}$$

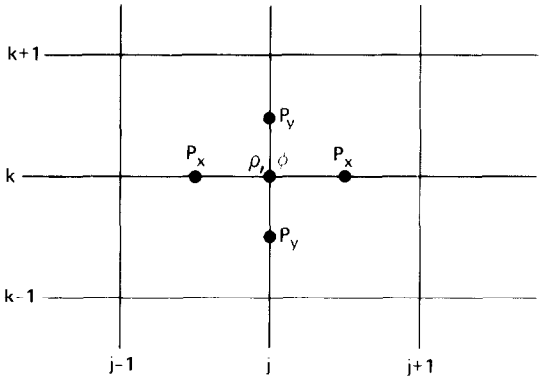

FIG. 1. Spatial grid, showing where ρ, ϕ, P_x, and P_y are defined; χ_x and χ_y are colocated with P_x and P_y.

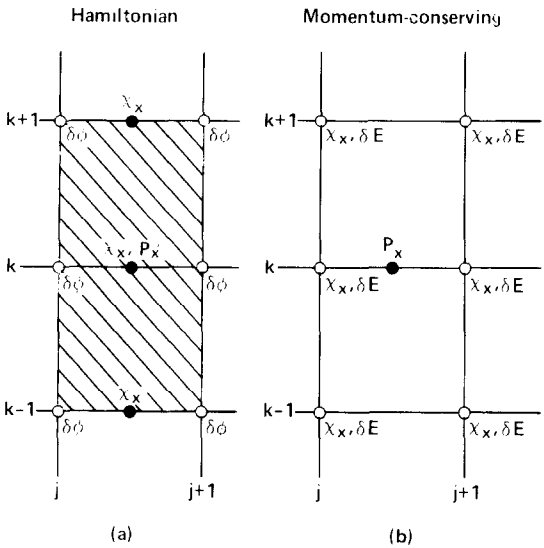

FIG. 2. For bilinear weighting ($m = 1$) the displacements δx_i for particles in two cells (hatched area) contribute to P_x (see (56)). In turn, these displacements are due to $\delta\phi$ at the circled grid points in Hamiltonian models (a), and $\delta\mathbf{E}$ at the same grid points in momentum-conserving models (b). Determination of P_x requires χ at only three locations for Hamiltonian (a) vs the six locations where $\delta\mathbf{E}$ is given in momentum-conserving models (b). The values of χ indicated in the figures are specific to the P_x at $(j + \frac{1}{2}, k)$. For P_x elsewhere, different χ's are required. However, the different χ's at any grid point depend on the same set of particle moments, and symmetries exist that further reduce the calculations, as can be deduced from Eq. (66).

where ρ_j is given by Eq. (46), and V_c is the volume of a cell. From Eq. (46) we find

$$\begin{aligned}\delta\rho_j &= -\sum_i q_i\,\delta\mathbf{x}_i\cdot\nabla S(\mathbf{X}_j-\mathbf{x}_i)\\ &= -V_c\sum_{j'}\delta\phi_{j'}\,\beta\,\Delta t^2\sum_i\frac{q_i^2}{m_i}\nabla S(\mathbf{X}_j-\mathbf{x}_i)]\cdot[\nabla S(\mathbf{X}_{j'}-\mathbf{x}_i)].\end{aligned}\tag{59}$$

If we express the particle sum in terms of an integral over density, then we can represent

$$\sum_i \beta\,\Delta t^2\frac{q_i^2}{m_i}\cdots \quad\text{by}\quad \int d\mathbf{x}\,\beta\omega_p^2(\mathbf{x})\,\Delta t^2\cdots=\int d\mathbf{x}\,\chi(\mathbf{x})\cdots$$

using (7). The equation for $\delta\phi_j$ is then

$$\rho_j^{(r)}+(\nabla^2\phi^{(r)})_j=-(\nabla^2\,\delta\phi)_j-\delta\rho_j \tag{60a}$$

$$=V_c\sum_{j'}\delta\phi_{j'}\int d\mathbf{x}[\nabla S(\mathbf{X}_j-\mathbf{x})]\cdot[\nabla S(\mathbf{X}_{j'}-\mathbf{x})][1+\chi(\mathbf{x})]. \tag{60b}$$

This equation is remarkably similar to the continuum result, Eq. (20).

There are some points to note: The sparsity of this matrix equation is the *same* as for the Laplacian alone. The matrix is symmetric, as is clear from the form of Eq. (59), and we show in Appendix B that the matrix is positive; these properties facilitate its numerical solution. To form the matrix, one must collect more information from the particle locations than in an explicit code, in which one needs only $\{\rho_j\}$.

The simplest example of this differencing is worth stating explicitly. Choosing linear-interpolation weighting for S, in one dimension we find

$$-\frac{1}{\Delta x}\left[(1+\chi_{j+1/2})\frac{\delta\phi_{j+1}-\delta\phi_j}{\Delta x}-(1+\chi_{j-1/2})\frac{\delta\phi_j-\delta\phi_{j-1}}{\Delta x}\right] \tag{61}$$

for the right-hand side of Eq. (60), with

$$\chi_{j+1/2}=\frac{1}{\Delta x}\sum_{i\in j+1/2}\beta\frac{q_i^2}{m_i}\Delta t^2 \tag{62}$$

in which the sum includes only particles in cell $j+1/2$ (i.e., $j\,\Delta x\leqslant x_i\leqslant(j+1)\,\Delta x$). This is a very simple and direct representation of Eqs. (19) and (20).

Referring to Eq. (61), we recognize that

$$P_{j+1/2}=-\chi_{j+1/2}\frac{\delta\phi_{j+1}-\delta\phi_j}{\Delta x}$$

for the linearly weighted Hamiltonian code, which is the same as we choose for simplified differencing in Section 3.4.

More generally, for one-dimensional spline weighting we can use the results of Section 4.1 to factor the difference operator in (60). Using (50) for $S'_m(X_j - x_i)$ we first find, in one dimension,

$$P_{j+1/2} = \Delta x \sum_{j'} \delta\phi_{j'} \sum_i \beta \frac{q_i^2}{m_i} \Delta t^2 \, S_{m-1}(X_{j+1/2} - x_i) \, S'_m(X_{j'} - x_i).$$

Using (50) for $S'_m(X_{j'} - x_i)$ then gives

$$P_{j+1/2} = -\sum_{j'} \chi_{j+1/2,j'+1/2} \frac{\delta\phi_{j'+1} - \delta\phi_{j'}}{\Delta x}, \tag{63}$$

where

$$\chi_{j+1/2,j'+1/2} = \sum_i \beta \frac{q_i^2}{m_i} \Delta t^2 \, \Delta x \, S_{m-1}(X_{j+1/2} - x_i) \, S_{m-1}(X_{j'+1/2} - x_i). \tag{64}$$

For linear weighting ($m = 1$), χ is nonzero only for $j' = j$.

In two dimensions with linear weighting we find

$$P_{x,j+1/2,k} = -\sum_{k'} \chi_{x,j+1/2,k,k'} \frac{\delta\phi_{j+1,k'} - \delta\phi_{j,k'}}{\Delta x} \tag{65}$$

with

$$\chi_{x,j+1/2,k,k'} = \frac{1}{\Delta x} \sum_i \beta \frac{q_i^2}{m_i} \Delta t^2 \, \Delta y \, S_1(Y_k - y_i) \, S_1(Y_{k'} - y_i), \tag{66}$$

where the sum is over only the particles in the hatched area of Fig. 2a, and χ is

4.3. *Standard Linear-Weighting Case*

We now construct the field solution algorithm corresponding to the most commonly used method for coupling the particles and grid. We refer to this as "momentum-conserving" because momentum is conserved (at least in an explicit code) whenever the field boundary conditions so indicate, e.g., in an open or periodic system [18, 26], but not in the presence of metallic boundaries.

Charge is collected using Eq. (46), as in the Hamiltonian codes. The Poisson equation and $\mathbf{E} = -\nabla\phi$ are solved by a variety of ad hoc spatially centered methods to obtain $\mathbf{E}$. The particle acceleration is then obtained from

$$\mathbf{a}_i = \frac{q}{m} V_c \sum_{j'} \mathbf{E}_{j'} S(\mathbf{X}_{j'} - \mathbf{x}_i) \tag{67}$$

rather than Eq. (58). Use of the same function S in field interpolation and charge collection, and location of all components of $\mathbf{E}$ at the same locations as ρ, are the keys to momentum conservation [18, 26].

4.3.1. *Susceptibility*

The calculation of $\delta\rho$ is given in Section 4.1. From Eq. (67) we obtain

$$\delta\mathbf{x}_i = \beta\,\Delta t^2\,\frac{q}{m}\,V_c \sum_{\mathbf{j}'} \delta\mathbf{E}_{\mathbf{j}'}\,S(\mathbf{X}_{\mathbf{j}'} - \mathbf{x}_i) \tag{68}$$

which we substitute into Eq. (49) for $\delta\rho$ to obtain

$$\begin{aligned}\delta\rho_{\mathbf{j}} &= -V_c \sum_{\mathbf{j}'} \delta\mathbf{E}_{\mathbf{j}'} \sum_i \beta\,\Delta t^2\,\frac{q_i^2}{m_i}\,S(\mathbf{X}_{\mathbf{j}'} - \mathbf{x}_i)\,\nabla S(\mathbf{X}_{\mathbf{j}} - \mathbf{x}_i) \\ &= \sum_{\mathbf{j}'} W_{\mathbf{j},\mathbf{j}'}\,\delta\mathbf{E}_{\mathbf{j}'}.\end{aligned} \tag{69}$$

This is used in the Poisson equation to obtain the field equation to be solved in a code. In one dimension, this is the result given in [3]. As noted there, $W_{\mathbf{j},\mathbf{j}'}$ is zero unless $|\mathbf{j}' - \mathbf{j}|\,\Delta x$ is smaller than the support of $S(\mathbf{x})$ (i.e., where $S \neq 0$), so the coupling does not extend far.

Some simplifications can be recognized through the use of Eqs. (51)–(52) when S is a spline function. Substituting (68) into (52) and reversing the order of summation,

$$\begin{aligned}P_{j+1/2} &= \sum_{j'} \delta E_{j'}\,\beta\,\Delta t^2 \sum_i \frac{q_i^2}{m_i}\,\Delta x\,S_m(X_{j'} - x_i)\,S_{m-1}(X_{j+1/2} - x_i) \\ &= \sum_{j'} \chi_{j+1/2,j'}\,\delta E_{j'},\end{aligned} \tag{70}$$

which is a convolution of δE and a (slightly) nonlocal susceptibility. For linear splines, $m = 1$, we have (see Eq. (53)),

$$\chi_{j+1/2,j'} = \sum_{i \in j+1/2} \beta\,\Delta t^2\,\frac{q_i^2}{m_i}\,S_1(X_{j'} - x_i). \tag{71}$$

Only two terms contribute, from $j' = j$ and $j + 1$:

$$P_{j+1/2} = \tfrac{1}{2}(\chi_{\mathrm{L},j}\,\delta E_j + \chi_{\mathrm{R},j+1}\,\delta E_{j+1}) \tag{72}$$

with $\frac{1}{2}\chi_{\mathrm{L},j} \equiv \chi_{j+1/2,j}$ and $\frac{1}{2}\chi_{\mathrm{R},j+1} \equiv \chi_{j+1/2,j+1}$.

4.3.2. *Field Solve in One Dimension*

We now set up the field equations in a form which has an obvious first integral. The one-dimensional field solve is commonly written as

$$\frac{\phi_{j+1} - 2\phi_j + \phi_{j-1}}{\Delta x^2} = -\rho_j, \tag{73a}$$

$$E_j = -\frac{\phi_{j+1} - \phi_{j-1}}{2\,\Delta x}. \tag{73b}$$

We solve instead for

$$E_{j+1/2} = -\frac{\phi_{j+1} - \phi_j}{\Delta x}, \tag{74}$$

with which the above field solve becomes

$$\frac{E_{j+1/2} - E_{j-1/2}}{\Delta x} = \rho_j, \tag{75a}$$

$$E_j = \frac{E_{j+1/2} + E_{j-1/2}}{2}. \tag{75b}$$

Using Eq. 51) the field equation is

$$(\delta E_{j+1/2} + P_{j+1/2}) - (\delta E_{j-1/2} + P_{j-1/2}) = \Delta x|\rho^{(r)} - \nabla \cdot E^{(r)}|_j.$$

This has a trivial first integral from which we obtain $D_{j+1/2} \equiv \delta E_{j+1/2} + P_{j+1/2}$. Now express P in terms of δE using (72) and (75b):

$$\begin{aligned} D_{j+1/2} &= \delta E_{j+1/2} + \tfrac{1}{4}[\chi_{\mathrm{L},j}(\delta E_{j-1/2} + \delta E_{j+1/2}) + \chi_{\mathrm{R},j+1}[\delta E_{j+1/2} + \delta E_{j+3/2})] \\ &= \tfrac{1}{4}\chi_{\mathrm{L},j}\,\delta E_{j-1/2} + [1 + \tfrac{1}{4}(\chi_{\mathrm{L},j} + \chi_{\mathrm{R},j+1})]\,\delta E_{j+1/2} + \tfrac{1}{4}\chi_{\mathrm{R},j+1}\,\delta E_{j+3/2}. \end{aligned}$$

This is a tridiagonal matrix equation for δE, which is easy to solve. Since $\chi \geqslant 0$, the matrix is positive and diagonally dominant.

If we solve for $\delta\phi$ instead of δE, and do not make use of the first integral, the field equation has a pentadiagonal matrix which is the product of three matrices, one of which is the tridiagonal matrix above.

4.3.3. *Another Form*

We can instead interpolate from the electric field at *half-integer* points $j + \frac{1}{2}$ (although momentum conservation is lost):

$$a_i = \frac{q}{m}\Delta x \sum_{j'} E_{j'+1/2} S_m(X_{j'+1/2} - x_i) \tag{76a}$$

$$= \frac{q}{m}\Delta x \sum_{j'} \left(\frac{\phi_{j'+1} - \phi_{j'}}{\Delta x}\right) S_m(X_{j'+1/2} - x_i). \tag{76b}$$

Using (52),

$$P_{j+1/2} = \sum_{j'} \chi_{j+1/2,j'+1/2}\, \delta E_{j'+1/2}, \tag{77}$$

where

$$\chi_{j+1/2,j'+1/2} = \beta\, \Delta t^2 \sum_i \frac{q_i^2}{m_i} \Delta x\, S_m(X_{j'+1/2} - x_i)\, S_{m-1}(X_{j+1/2} - x_i). \tag{78}$$

For linear weighting, this χ is nonzero for $j' = j$ and $j \pm 1$. Although χ is more strongly local than in the preceding case, the field equations remain tridiagonal for $\delta\mathbf{E}$ or pentadiagonal for $\delta\phi$.

4.3.4. *Field Solve in Two Dimensions*

In two (or three) dimensions we are not able to make such a simple integration of the field equation. Use of the polarization vector $\mathbf{P}$ and (26) still helps us set up the difference equations. In order to form P_x, P_y at grid points $(j \pm \frac{1}{2}, k)$, $(j, k \pm \frac{1}{2})$, and thence $\delta\rho_{j,k}$, we need $\delta\mathbf{E}$ at adjacent grid points (j, k), $(j \pm 1, k)$, and $(j, k \pm 1)$. In the usual scheme with centered differencing of ϕ, this would require $\delta\phi$ from all the neighboring grid points and would therefore couple $\delta\phi$ at 21 grid points. This can be seen by rotating the pattern in Fig. 2 by 90 degrees to account for $P_{y,j,k+1/2}$, $P_{x,j-1/2,k}$, and $P_{y,j,k-1/2}$. These require δE_x and δE_y at the nine grid points shown in Fig. 2. In turn, these fields require $\delta\phi$ at the 9 grid points shown, plus three additional grid points on each of the four sides, accounting for the total of 21.

4.4. *Convergence of the Iteration Including Grid Effects*

In Section 3.6 we examined the convergence of iterative solution of the implicit field equation in the absence of spatial differencing effects. We calculated the ratio $|\rho^{(r+1)} - \nabla \cdot \mathbf{E}^{(r+1)}|/|\rho^{(r)} - \nabla \cdot \mathbf{E}^{(r)}|$, and found that the numerator vanishes through linear order in $\delta\mathbf{x}^{(r+1)} \cong \beta\, qm^{-1}\, \Delta t^2\, \delta\mathbf{E}^{(r+1)}$ for *consistent* representations of $\delta\mathbf{x}^{(r+1)}$ and $\chi^{(r)}$ (see Eqs. (37) and (39)). This follows directly from the construction of the implicit field solution. However, there are some qualifications.

When a particle crosses a cell boundary as a result of the increment $\delta\mathbf{x}$ and linear weighting is in use, the resulting $\delta\rho$ due to this particle is not linear in $\delta\mathbf{x}$ even to leading order, but is piecewise linear. With "subtracted dipole" weighting [27], $\delta\rho$ is *discontinuous*, vitiating the linearization. The number of particles which cross is proportional to $\delta\mathbf{x}$ and the number density. When higher-order spline weighting is used, the linearization is more accurate in that $\partial S/\partial x$ is continuous; however, $\delta\rho$ now includes small terms quadratic in $\delta\mathbf{x}$. All these nonlinearities are omitted in both direct and moment implicit field predictions. The resulting error can be reduced by linearization with respect to an improved prediction of the orbit, obtained using $\mathbf{E}_{n+1}^{(0)} = \mathbf{E}_n$ instead of 0, for example (Section 3.2).

When simplified differencing is used, such as in Section 3.4, two additional types of

errors can occur that contribute to $|\rho^{(r+1)} - \nabla \cdot \mathbf{E}^{(r+1)}|$. The first was encountered already in the gridless case (Section 3.6) and arises from the inconsistency of $\chi^{(r)}$ and the equations of motion leading to $\delta\mathbf{x}^{(r+1)}$ and $\rho^{(r+1)}$. The other error is due to the different representations of $\chi^{(r)}$ and $\nabla \cdot \chi\mathbf{E}$ on the spatial grid in strict and simplified schemes. A loss of convergence results that is very similar to that suffered with inconsistent spatial smoothing, and the analysis is similar to that of Section 3.6. With a representative calculation like that leading to Eqs. (36) and (40), we obtain

$$\frac{|\rho^{(r+1)} - \nabla \cdot \mathbf{E}^{(r+1)}|}{|\rho^{(r)} - \nabla \cdot \mathbf{E}^{(r)}|} = \frac{|\{\nabla \cdot \chi^{(r)}\, \delta\mathbf{E}^{(r+1)}\}' - \nabla \cdot \chi^{(r)}\, \delta\mathbf{E}^{(r+1)}|}{|\nabla \cdot (1+\chi^{(r)})\, \delta\mathbf{E}^{(r+1)}|} \tag{79}$$

to leading order, where $\nabla \cdot \chi\, \delta\mathbf{E}$ is a representation using strict differencing, and $\{\cdots\}'$ indicates the simplified-differencing form.

An instructive example is furnished by considering the simplified scheme in Section 3.4 and the strictly differenced scheme of Section 4.3. The numerator of (79) is due to the difference between the two evaluations of $\delta\rho = -\nabla \cdot \mathbf{P} = -\nabla \cdot \chi\, \delta\mathbf{E}$. For the simplified scheme in one dimension, (27) and (74) give

$$P_{j+1/2} = -\chi_{j+1/2} \frac{\delta\phi_{j+1} - \delta\phi_j}{\Delta x} = \chi_{j+1/2}\, \delta E_{j+1/2},$$

and $\chi_{j+1/2}$ is specified by (28). For linear charge weighting the strictly differenced scheme uses, from (72) and (75b),

$$P_{j+1/2} = \tfrac{1}{4}\chi_{\mathrm{L},j}(\delta E_{j+1/2} + \delta E_{j-1/2}) + \tfrac{1}{4}\chi_{\mathrm{R},j+1}(\delta E_{j+1/2} + \delta E_{j+3/2}).$$

The charge density increment in both cases is $\delta\rho = -(P_{j+1/2} - P_{j-1/2})/\Delta x$, which involves $\delta E_{j+1/2}$ and $\delta E_{j-1/2}$ in the simplified scheme and $\delta E_{j-3/2}$, $\delta E_{j-1/2}$, $\delta E_{j+1/2}$, and $\delta E_{j+3/2}$ for strict differencing.

Thus, both the difference in definitions of χ and the different stencils on δE contribute to the numerator of (79) and hence slow the convergence. Rapid variations in plasma density lead to a loss of convergence through the difference in susceptibilities. Spatial smoothing may help here. Perhaps tuning of the form of $\chi_{j+1/2}$ will improve convergence of simplified methods. Even in a uniform plasma, the different electric field stencils cause a loss of convergence at short wavelengths. Currently we are studying the effect of incomplete convergence on stability.

Thus, superlinear convergence is lost with simplified differencing, and convergence in simulations with rapid fluctuations or gradients in plasma density is apt to be slower. Spatial smoothing helps; Barnes *et al.* [9] find that, with consistent spatial smoothing, simulations with simplified differencing behave well.

4.5. *Strict versus Simple Differencing*

Here we compare convergence and computational complexity for strict and simple spatial differencing.

With strict spatial differencing and consistent spatial smoothing, convergence to solutions of the field + particle equations is limited only by the magnitude of $(q\,\Delta t^2/m)(\partial E/\partial x)$, not by finite differencing or particle weighting errors.

In Section 4.3.4 we outlined the derivation of a two-dimensional field equation in which 21 grid points were coupled. These matrix coupling coefficients and ρ require accumulation on the grid of eight independent quantities from the particles: the particle moments $\{1, x, y, xy, x^2, y^2, xy^2, x^2y\}$ calculated with respect to the cell centers, or the equivalent. Note that the first four moments are equivalent to the charge density which must be calculated in any case.

The Hamiltonian solve is much simpler, with only nine grid points coupled and requiring the equivalent of accumulation of six different quantities from the particles: $\{1, x, y, xy, x^2, y^2\}$. Furthermore, the symmetries of the Hamiltonian χ in Eq. (66), and hence the symmetry of the matrix field equation, allow reduction of the data to be accumulated from the particles to five quantities at each grid point.

These formulations have been systematically derived, strictly following rules for performing spatial differences, in order to have good convergence properties, but require considerably more data from the particles than the ad hoc scheme in Section 3.4.

5. Summary and Future Directions

This paper has examined in detail the formulation and structure of an implicit algorithm for solving the coupled particle equations of motion and Poisson equation for the electrostatic field. Some of the important contributions of this work are as follows. We systematically derived direct implicit particle simulation schemes in general and provided specific examples in one and two dimensions. Our algorithms use particle data directly without introducing fluid moment equations and significantly relax the time-step constraints of conventional particle simulation schemes. Demonstration and application of these methods were described elsewhere [3, 9]. Addressed here for the first time is the convergence of the necessarily approximate implicit solution of the coupled field and particle equations. We considered the remaining restrictions on Δt. Although $\omega_{pe}\,\Delta t \gg 1$ is allowed, accuracy (but not stability) of particle trajectories and the plasma collective response requires $|kv\,\Delta t| \lesssim 1$, and resolution of particle trajectories and accurate solution of the coupled field and particle equations lead to the constraint $\omega_{tr}\,\Delta t \lesssim 1$.

A number of topics for continued research in this area immediately come to mind. We have begun to construct a direct implicit electromagnetic algorithm. Further research should examine the potential for and limitations of simplified differencing in both the direct implicit and implicit moment methods. For example, we have a demonstration of superlinear convergence only for *strict* differencing with *consistent* smoothing and with inclusion of the Newton-Raphson correction to χ. Convergence with simplified differencing is slower at short wavelengths $\cong \Delta x$, for large field gradients, and for sharply varying density profiles. It is conceivable that these wavelengths may remain stable nonetheless due to phase mixing (density pertur-

bations decay ballistically as $\exp(-\frac{1}{2}k^2v_t^2t^2)$ [28]). We have learned how to alter the algorithm to obtain exact momentum conservation, with strict *or* simplified differencing, without iteration.

We have begun to analyze the linear dispersion relation and stability of oscillations including the effects of inconsistent spatial smoothing, ad hoc differencing, and use of $\mathbf{E}_n$ and other first predictions for $\mathbf{E}_{n+1}^{(0)}$. We find a connection between the modification of the dispersion relation and the loss of convergence as calculated in Sections 3.6 and 4.4. Numerical stability can be compromised, especially at short wavelengths. However, the analysis also suggests ways of performing inconsistent spatial smoothing and ad hoc differencing that preserve stability. Convergence and linear dispersion properties can guide the design and use of new schemes.

Additional computational savings may be accrued by combining direct implicit solution of the field and particle equations with sub-cycling [5] or orbit-averaging [6, 7], in which one or more particle species are advanced over many small time steps with implicitly predicted fields that evolve on a longer time scale. Experience with implicit algorithms will undoubtedly suggest other research topics.

APPENDIX A: Relation Between Implicit Moment and Direct Implicit Methods

Here we compare and contrast the "direct" and "moment" approaches to implicit particle-in-cell plasma simulation. In the implicit moment method [1, 2] the time-advanced charge density is expressed using velocity moment equations, which are closed by accumulating a flux and stress tensor from particles at the *known* time level n. The electric field is at the advanced time level. An elementary version of the implicit moment equation method is

$$\mathbf{j}'_{n+1/2} = \mathbf{J}_{n-1/2} - \frac{q\,\Delta t}{m}(\nabla \cdot \mathbf{P}_n - \rho_n \mathbf{E}_n), \tag{A.1}$$

$$\nabla \cdot \mathbf{E}_{n+1} = \rho'_{n+1} \cong \rho_n - \Delta t\, \nabla \cdot \mathbf{j}'_{n+1/2}, \tag{A.2}$$

where $(\rho, \mathbf{J}, \mathbf{P}) \equiv n\langle q, q\mathbf{v}, m\mathbf{v}\mathbf{v}\rangle$ are formed as sums over *known* particle coordinates, while $(\mathbf{j}', \rho')$ are fluid quantities. Eliminating $\mathbf{j}'_{n+1/2}$,

$$\nabla \cdot \mathbf{E}_{n+1} + \frac{q}{m}\Delta t^2\, \nabla \cdot (\rho_n \mathbf{E}_{n+1}) = \rho_n - \Delta t\, \nabla \cdot \left(\mathbf{J}_{n-1/2} - \frac{q\,\Delta t}{m}\nabla \cdot \mathbf{P}_n\right). \tag{A.3}$$

To explain the relationship between the direct and moment approaches, Mason observed that the right-hand side is equal to a field-free extrapolation of the charge density obtained by setting $\mathbf{E}_{n+1} = 0$ in Eq. (A.1), and therefore corresponds to the charge density $\rho_{n+1}^{(0)}$ in (8) or (9) which was formed from the positions $\{\tilde{\mathbf{x}}_{n+1}\}$ obtained from the particle equations of motion with $\mathbf{E}_{n+1}$ set to zero. The other

difference between (A.3) and (8) is that the susceptibility term in (8) uses particle positions at time $n+1$ while the analogous term in (A.3) uses positions at time n.

Thus, the implicit moment and the direct implicit methods can be closely related. Of course, important differences persist. For example, collection of the stress tensor $\mathbf{P}$ from known data leads to a stability constraint $kv_t \Delta t \lesssim 1$ that does not arise in our direct method. We believe that the particle equations themselves are a better guide to the particles' field-free motion, and therefore to the right hand side of (A.3), than are moment equations.

As with our Section 3.4, in differencing the implicit moment equations, consistency with the particle force calculation is not attempted. When such consistency is not required, the direct method provides a simpler field equation and requires less computational work for the particles. If strong convergence to solutions of the field + particle equations is desired, we provide in Sections 3 and 4 a systematic expansion procedure that leads naturally both to a strict differencing scheme with consistent spatial smoothing for which convergence is most conservatively expected, and to a straightforward iteration procedure.

APPENDIX B: POSITIVITY OF THE FIELD MATRIX EQUATIONS

To show that the matrix operator in the field equation for the Hamiltonian model is a positive matrix, multiply the right-hand side of (60a) by $V_c\,\delta\phi_j$ and sum over $\mathbf{j}$. Using (59),

$$V_c \sum_{\mathbf{j}} \delta\phi_j[-(\nabla^2\,\delta\phi)_j - \delta\rho_j]$$

$$= -V_c \sum_{\mathbf{j}} \delta\phi_j(\nabla^2\,\delta\phi)_j + \sum_i \beta\,\Delta t^2 \frac{q_i^2}{m_i}\left[\nabla V_c \sum_{\mathbf{j}} \phi_j S(\mathbf{X}_j - \mathbf{x}_i)\right]^2.$$

The particle term is positive for any $\delta\phi$; therefore the matrix is positive if the representation of $-\nabla^2$ is positive. To show positivity when (57) is used for the Laplacian and to make connection to the continuum case, we write the particle sum as an integral, as in Eq. (60b). Denoting the field solve matrix by A, we obtain

$$V_c\,\delta\phi^T A\,\delta\phi = \int d\mathbf{x}\left[\nabla V_c \sum_{\mathbf{j}} \delta\phi_j S(\mathbf{X}_j - \mathbf{x})\right]^2 [1+\chi] \geqslant 0 \tag{B.1}$$

if $1+\chi(\mathbf{x}) > 0$ everywhere, as is the case when χ is given by (7). When χ is a tensor, as in the magnetized case (Section 3.7), only the symmetric part contributes. Equation (B.1) is a direct analogue to the continuum result,

$$-\int_V dx\,\phi\nabla\cdot[1+\chi]\,\nabla\phi = \int_V d\mathbf{x}[\nabla\phi]^2[1+\chi] - \int_S \mathbf{ds}\cdot(1+\chi)\,\phi\nabla\phi. \tag{B.2}$$

Note that $1+\chi$ may become negative if the Newton–Raphson correction of Appendix C is used.

The simplified algorithm of Section 3.4 also leads to a positive matrix. The field solve matrix A is given in one dimension by (61) but now we say nothing more about χ than that $1+\chi>0$. Multiply (61) by $\Delta x\,\delta\phi_j$ and sum to form the inner product

$$\Delta x\,\delta\phi^T A\,\delta\phi = -\sum_j \delta\phi_j(1+\chi_{j+1/2})\frac{\delta\phi_{j+1}-\delta\phi_j}{\Delta x} + \sum_j \delta\phi_j(1+\chi_{j-1/2})\frac{\delta\phi_j-\delta\phi_{j-1}}{\Delta x} \tag{B.3a}$$

$$= \Delta x\sum_j (1+\chi_{j+1/2})\left(\frac{\delta\phi_{j+1}-\delta\phi_j}{\Delta x}\right)^2 \geqslant 0. \tag{B.3b}$$

In the second sum in (B.3a) we have redefined index j as $j+1$, then combined the two sums term by term to obtain (B.3b) (plus boundary terms which are commonly zero). This result is directly analogous to (B.2). In addition to being positive, the matrix is an "M-matrix," i.e., all off-diagonal elements are <0. This is obvious from (61) in one dimension, and is true also in two dimensions.

To show that the matrix for the strict, linear-weighting case (Section 4.3) is positive we proceed similarly, using (51), (70)–(71), and (73b),

$$\Delta x\sum_j \delta\psi_j(\nabla\cdot\chi\nabla\,\delta\phi)_j = \Delta x\sum_j \delta\psi_j\frac{P_{j+1/2}-P_{j-1/2}}{\Delta x}$$

$$= \Delta x\sum_j\sum_{j'}\frac{1}{2}(\chi_{j+1/2,j'}+\chi_{j+1/2,j'+1})\left(\frac{\delta\psi_{j+1}-\delta\psi_j}{\Delta x}\right)\left(\frac{\delta\phi_{j'+1}-\delta\phi_{j'}}{\Delta x}\right), \tag{B.4}$$

where

$$(\chi_{j+1/2,j'}+\chi_{j+1/2,j'+1})$$

$$= \beta\,\Delta t^2\sum_i \frac{q_i^2}{m_i}\Delta x[S_m(X_{j'}-x_i)+S_m(X_{j'+1}-x_i)]\,S_{m-1}(X_{j+1/2}-x_i)$$

is positive when S is a spline function, as here.

In the second linear-weighting form, where the acceleration is interpolated from $\delta E_{j+1/2}=-(\delta\phi_{j+1}-\delta\phi_j)/\Delta x$, we find from (77)

$$\Delta x\sum_j \delta\psi_j(\nabla\cdot\chi\nabla\,\delta\phi)_j = \Delta x\sum_j\sum_{j'}\chi_{j+1/2,j'+1/2}\left(\frac{\delta\psi_{j+1}-\delta\psi_j}{\Delta x}\right)\left(\frac{\delta\phi_{j'+1}-\delta\phi_{j'}}{\Delta x}\right). \tag{B.5}$$

With χ given by (78), we see this is positive.

Although (43) is neutral in its effect on positivity of the field equation, a straightforward central differencing of the antisymmetric terms arising when the plasma is magnetized results in a loss of positivity [29]. The differencing of antisymmetric terms is dealt with in [30].

In summary, in each case the matrix is positive if $\chi>0$. For the simplified and the

Hamiltonian cases, the matrix is also symmetric. These properties are helpful to iterative solution of the field equation in two dimensions, where direct solution methods are often impractical.

APPENDIX C: NEWTON–RAPHSON CORRECTION TO PARTICLE POSITION

In Section 3.5.2 we showed there is a limitation on $\Delta t^2\, \partial E/\partial x$ due to an approximation used in evaluating δx. Here we reopen this question, to see the effect on our finite-difference field solution of using the more accurate Newton–Raphson solution for δx, Eq.(37). Since $N_{j+1/2} = [1 - (\beta q\, \Delta t^2/m)\, \partial E/\partial x]_{j+1/2}$ is constant within a cell, for linear weighting, this factor may be removed from the particle sum for each species.

$$\frac{1}{2}\chi_{\mathrm{L},j} = (\beta/N_{j+1/2})\frac{q^2}{m}\Delta t^2 \sum_{i \in j+1/2} S_1(X_j - x_i),$$

$$\frac{1}{2}\chi_{\mathrm{R},j+1} = (\beta/N_{j+1/2})\frac{q^2}{m}\Delta t^2 \sum_{i \in j+1/2} S_1(X_{j+1} - x_i).$$

It is very convenient that the denominator does not need to be accumulated for each particle, but is added to χ later. However, there are several awkward features. The field equation becomes nonlinear. In two or three dimensions this factor becomes a matrix operation. This correction can cause $1 + \chi$ to become negative, which affects the solution of the field equations (Appendix B). In short, we do not recommend use of this Newton-Raphson factor, nor do we know anyone who has.

ACKNOWLEDGMENTS

It is a pleasure to acknowledge valuable conversations with D. Barnes, J. Byers, J. Denavit, and R. J. Mason. This collaboration was a result of a workshop on implicit methods organized principally by C. K. Birdsall. This work was performed under the auspices of the U.S. Department of Energy, by the Lawrence Livermore Laboratory under Contract No. W-7405-Eng-48.

REFERENCES

1. R. J. MASON, *J. Comput. Phys.* **41** (1981), 233.
2. J. DENAVIT, *J. Comput. Phys.* **42** (1981), 337.
3. A. FRIEDMAN, A. B. LANGDON, AND B. I. COHEN, *Comm. Plasma Phys. Controlled Fusion* **6** (1981)
6. B. I. COHEN, T. A. BRENGLE, D. B. CONLEY, AND R. P. FREIS, *J. Comput. Phys.* **38** (1980), 45.
7. B. I. COHEN, R. P. FREIS AND V. THOMAS, *J. Comput. Phys.* **45** (1982), 345.
8. B. I. COHEN, A. B. LANGDON, AND A. FRIEDMAN, *J. Comput. Phys.* **46** (1982), 15.

9. D. C. BARNES. T. KAMIMURA, J.-N. LEBOEUF, AND T. TAJIMA, "Implicit Particle Simulation of Magnetized Plasmas," Report IFSR #68, Institute for Fusion Studies, University of Texas at Austin, September, 1982; *J. Comput. Phys.*, to appear.
10. R. J. MASON, *Phys. Rev. Lett.* **47** (1981), 652.
11. D. W. FORSLUND AND J. U. BRACKBILL, *Phys. Rev. Lett.* **48** (1982), 1614.
12. J. U. BRACKBILL AND D. W. FORSLUND, *J. Comput. Phys.* **46** (1982), 271.
13. D. O. DICKMAN, R. L. MORSE, AND C. W. NIELSON, *Phys. Fluids* **12** (1969), 1708.
14. C. W. NIELSON AND H. R. LEWIS, *in* "Methods in Computational Physics" (B. Alder, S. Fernbach, and M. Rotenberg, Eds., J. Killeen, Vol. Ed.), p. 367, Academic Press, New York, 1976; see Eqs. (11b) and (25).
15. A. FRIEDMAN, R. L. FERCH, R. N. SUDAN, AND A. T. DROBOT, *Plasma Phys.* **19** (1977), 1101; A. MANKOFSKY, A. FRIEDMAN, AND R. N. SUDAN, *Plasma Phys.* **23** (1981), 521.
16. A. B. LANGDON AND B. F. LASINSKI, *in* "Methods in Computational Physics" (B. Alder, S. Fernbach, and M. Rotenberg, Eds., J. Killeen, Vol. Ed.), p. 327, Academic Press, New York, 1976.
17. A. B. LANGDON, *Phys. Fluids* **22** (1979), 163.
18. A. B. LANGDON, *J. Comput. Phys.* **6** (1970), 247.
19. A. B. LANGDON AND C. K. BIRDSALL, *Phys. Fluids* **13** (1970), 2115.
20. J. M. DAWSON, *in* "Methods in Computational Physics" (B. Alder, S. Fernbach, and M. Rotenberg, Eds.), p. 1, Academic Press, New York, 1970.
21. J. S. CHANG AND G. COOPER, *J. Comput. Phys.* **6** (1970), 1.
22. H. SAKAGAMI, K. NISHIHARA, AND D. COLOMBANT, "Stability of Time-Filtering Particle Code Simulation," Institute of Laser Engineering Report ILE8117P, August 10, 1981.
23. O. BUNEMAN, *J. Comput. Phys.* **1** (1967), 517.
24. D. C. BARNES AND T. KAMIMURA, "LOMEGA: A Low Frequency, Field Implicit Method for Plasma Simulation," Institute of Plasma Physics, IPPJ-570, Nagoya University, April 1982.
25. A. B. LANGDON, *J. Comput. Phys.* **12** (1973), 247.
26. C. K. BIRDSALL AND A. B. LANGDON, "Plasma Physics Via Computer Simulation," McGraw–Hill, New York, 1983.
27. W. L. KRUER, J. M. DAWSON, AND B. ROSEN, *J. Comput. Phys.* **13** (1973), 114.
28. J. N. HAYES, *Phys. Fluids* **4** (1961), 1387; R. C. DAVIDSON, "Methods in Nonlinear Plasma Theory," Sect. 8.6, Academic Press, New York, 1972.
29. N. V. PEALE, "The Power of Positive Thinking," Prentice–Hall, New York, 1952.
30. J. PERT, *J. Comput. Phys.* **42** (1981), 20; see pp. 28–30.